Wavelength Division Multiplexing in Visible Light Communications Using Fluorescent Fiber Antennas

Cuiwei He[®], Member, IEEE, Yuru Tang[®], Chen Chen[®], Senior Member, IEEE, and H. Y. Fu[®], Senior Member, IEEE

Abstract—The use of fluorescent antennas in visible light communications (VLC) can significantly enhance the transmission performance by providing both a high optical concentration gain and a wide field of view (FOV) without being constrained by étendue. Moreover, as these antennas have the function of optical filtering, they can be used for supporting wavelength-division multiplexing (WDM) to boost the transmission data rate. However, there are several notable challenges when fluorescent antennas are used in WDM transmission. One challenge is that, due to the relatively wide absorption spectra of the fluorophores, the signal transmitted from different light sources can often only be partially separated in the optical domain. This causes crosstalk between different channels and consequently, the transmitted signals need to be further separated in the electrical domain. Another challenge arises from the performance imbalance among different decoded data streams, mainly caused by the differences in the frequency response between different transmitters. To address the first challenge, this paper introduces a new channel estimation method which enables the effective acquisition of the channel matrix for each orthogonal frequency-division multiplexing (OFDM) subcarrier without encountering interference. Thus, the signal separation step can be implemented more successfully in the frequency domain. Moreover, to overcome the imbalance between the data streams transmitted by different transmitters, we incorporate pairwise coding (PWC) into the system. Its performance was demonstrated via a WDM VLC testbed in which different colors of light-emitting diodes (LEDs) are configured to transmit independent data and commercially available fluorescent fibers are used to construct the optical antennas. Taking into account practical indoor illumination needs, we measured the system's performance across different illuminance levels. The results show that the use of PWC can well balance the performance between different channels, always leading to significant transmission data rate improvement.

Index Terms—Fluorescent antennas, LEDs, pairwise coding, visible light communications, wavelength division multiplexing.

Manuscript received 18 October 2023; revised 3 January 2024 and 28 January 2024; accepted 4 February 2024. Date of publication 7 February 2024; date of current version 16 May 2024. The work was supported by the Japan Society for the Promotion of Science (JSPS) Kakenhi under Grant JP 23K13332. (Corresponding authors: Cuiwei He; Chen Chen.)

Cuiwei He is with the School of Information Science, Japan Advanced Institute of Science and Technology, Ishikawa 923-1211, Japan (e-mail: cuiweihe@jaist.ac.jp).

Yuru Tang and H. Y. Fu are with Tsinghua Shenzhen International Graduate School, Tsinghua University, Shenzhen 518055, China, and also with Peng Cheng Laboratory, Shenzhen 518055, China (e-mail: tyr23@mails.tsinghua.edu.cn; hyfu@sz.tsinghua.edu.cn).

Chen Chen is with the School of Microelectronics and Communication Engineering, Chongqing University, Chongqing 400044, China (e-mail: c.chen@cqu.edu.cn).

Color versions of one or more figures in this article are available at https://doi.org/10.1109/JLT.2024.3363164.

Digital Object Identifier 10.1109/JLT.2024.3363164

I. INTRODUCTION

ISIBLE light communication (VLC) is an emerging technology with the potential to play a significant role in future wireless networks [1], [2]. Like all other communication systems, the transmission performance of a VLC link is highly dependent on the signal-to-noise ratio (SNR) at the receiver's output. A common method to enhance the SNR in VLC is by placing a concentrating lens in front of the photodetector. However, using a lens can result in a relatively bulky receiver structure. More importantly, the conservation of étendue implies that a high optical gain results in a narrower field of view (FOV) [3]. This means that the performance of many VLC systems is more susceptible to misalignment between the transmitter and the receiver in comparison to their radio frequency (RF) counterparts.

Recent research in the development of optical antennas incorporating fluorophores has shown many promising results for building VLC receivers with compact structures and wide FOVs [4], [5], [6], [7], [8], [9], [10], [11], [12], [13], [14], [15]. The structure of these optical antennas consists of a fluorescent light emitting layer and a cladding layer. Firstly, as fluorophores selectively absorb specific wavelengths of light, these antennas are capable of optical filtering. Additionally, thanks to the presence of the cladding layer, many emitted photons can be guided to the antenna's edge where a photodetector is positioned. The relatively large light-collecting area of the antenna means that the amount of light received by the photodetector can be increased, consequently, the SNR of the transmission can be enhanced. Moreover, because their light concentration is based on fluorescence, these antennas are not constrained by étendue, enabling them to achieve both a high concentration gain and a wide FOV. Another important advantage of employing fluorescent antennas is the short photoluminescence (PL) lifetime of the selected fluorophores. This characteristic allows them to respond fast to the changes in the received light intensity, thus supporting a very high transmission bandwidth [16].

In addition to the above mentioned benefits, the selective wavelength absorption property of fluorophores means that these antennas can be used to support wavelength division multiplexing (WDM) for boosting the transmission data rate [17], [18]. This involves constructing a transmitter with multiple light sources for sending independent data streams and a receiver with multiple fluorophores with each selectively absorbing the light emitted from a specific light source. For example, in [17],

0733-8724 © 2024 IEEE. Personal use is permitted, but republication/redistribution requires IEEE permission. See https://www.ieee.org/publications/rights/index.html for more information.

a specially designed fluorescent antenna incorporating two fluorescent layers made of different organic dyes was explored to support WDM, with the light sources being a blue light-emitting diode (LED) and a green LED. Meanwhile, commercially available fluorescent fibers were utilized to establish WDM links within a laser-based underwater optical wireless communication (OWC) system [18]. Despite the many advantages of using fluorescent antennas for supporting WDM transmission, one particular challenge shared by these pioneering studies is that, due to the relatively wide absorption spectra of the fluorophores, crosstalks between different channels can hardly be avoided.

To mitigate the crosstalk effect, both [17] and [18] treat the channel as a matrix, with each of its elements representing the optical channel gain associated with different transmitters and detectors, and subsequently multiply the inverse of this channel matrix with the received signals. However, solely focusing on optical power for constructing the channel matrix means that this matrix is independent of the frequency of the transmitted signal, and therefore, the transmission data rate. Furthermore, the feasibility of computing the inverse of the channel matrix relies on whether the channel matrix is well-conditioned or not. As a result, this approach may lead to only partial signal separation. This issue is less noticeable with on-off keying (OOK) modulation which is considered in both [17] and [18]. However, it becomes obvious when employing orthogonal frequency division multiplexing (OFDM) modulation, which is now widely acknowledged as the preferred modulation scheme in the VLC standard [19]. This is because, when OFDM is used, the low-pass frequency response of the electrical channel would lead to different channel coefficients for different OFDM subcarriers. As a result, the channel matrix varies across different subcarriers. In this case, to more accurately separate the signals transmitted from different light sources, the separation step should be carried out individually for each subcarrier. Moreover, even with a signal separation step implemented, the different light sources used in WDM, either lasers or LEDs, often possess distinct frequency responses and bandwidths. This discrepancy can result in significant performance imbalance among different channels. Similar to various other multiplexing techniques, such as multiple-input and multiple-output (MIMO), the overall system's performance is often dominated by the data stream decoded with the worst performance [20]. Therefore, it is crucial to employ suitable digital signal processing (DSP) algorithms which can balance performance across the different channels.

In this study, we build a WDM VLC system utilizing LEDs as data transmitters and fluorescent fibers to create optical antennas. Both the LEDs and the fibers are commercially available products. At the transmitter, RGB LEDs are employed to generate white light which is suitable for indoor illumination. At the receiver, we choose the fluorescent fibers manufactured by Kuraray to construct the optical antennas. At the current moment, as only blue absorption and green absorption fibers are available on the market, the blue LED and the green LED are configured to transmit two independent data streams, while the red LED is powered with a DC current. First, we show that, through careful selection of suitable fluorescent fibers, we can create a WDM system with its channel being as a triangular matrix which has better conditions compared to those in [17]

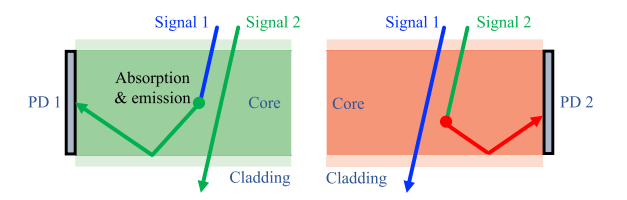


Fig. 1. Schematic diagram to show the use of fluorescent antennas for WDM.

and [18]. Moreover, instead of considering the channel matrix only derived from optical power, we take into account the electrical-to-electrical channel gain in constructing the channel matrix. Additionally, we consider OFDM modulation and the signal separation is implemented on each OFDM subcarrier so that the effects of the low-pass frequency response are taken into consideration. Furthermore, to obtain the channel matrix of each OFDM subcarrier, we introduce a new channel estimation technique designed specifically for this WDM-OFDM system. This technique is very effective but simple to implement. Also, this work makes a significant contribution by demonstrating that, owing to the distinct frequency responses between different LED transmitters, the decoded data streams exhibit a notable imbalance in performance. To overcome this imbalance problem, we integrate pairwise coding (PWC) [21], [22], a technique previously demonstrated to effectively enhance the performance of various multiplexing systems facing performance imbalances, including MIMO [23] and polarization-division multiplexing [24]. In the experiment, we measured the system's performance under varying illuminance levels, both with and without PWC. The measured results show that, when the illuminance level is relatively low, the use of PWC can double the achievable transmission data rate. While the illuminance level is high, the use of PWC can also increase the data rate by 25%.

The rest of the paper is organized as follows. Section II explains both the channel crosstalk and imbalance problems by discussing the spectra of the LEDs, the spectra of the fluorophores and the channel frequency responses. Section III then introduces the details of the PWC encoder and decoder that are incorporated into our system. This is followed in Section IV by a description of our new channel estimation method. Section V describes our experimental setup. Then, the measured results, including the concentration gain, the channel response, the signal constellations, and the measured bit error rates (BERs), are presented in Section VI. Finally, Section VII concludes the paper.

II. A FLUORESCENT ANTENNA BASED WDM SYSTEM

In this section, we highlight the transmission crosstalk and the channel imbalance problems in a fluorescent antenna based WDM system by using our selected LED transmitters and fluorescent fibers as examples.

A. Fluorescent Antenna

To illustrate how a fluorescent antenna works, Fig. 1 shows some possible light paths when photons pass through the antenna. Since the fluorophore selectively absorbs specific

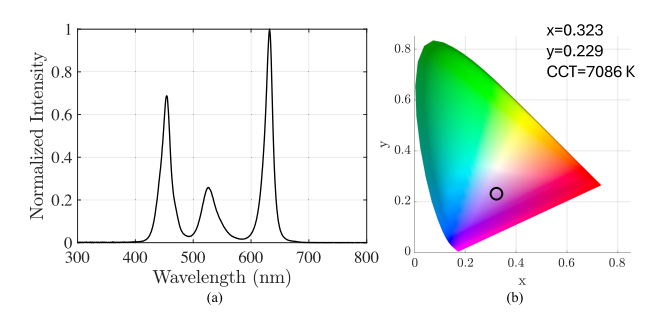


Fig. 2. (a) Spectrum of the RGB LED luminaire, (b) associated CIE coordinates.

wavelengths of light, the incident light outside the absorption spectrum would pass directly through the antenna without being absorbed. Alternatively, if the light falls within the absorption spectrum, the photons can be absorbed by the fluorophore. The absorption of a photon may be relaxed non-radiatively or result in the emission of a photon with a longer wavelength in a random direction. In this case, through total internal reflection, many emitted photons can be waveguided towards the antenna's edge, where a photodetector is positioned. Because the fluorescent antenna is designed with a much larger surface area compared to the size of the photodiode, its use can usually increase the number of detected photons and therefore the SNR at the receiver output. Moreover, since étendue is not conserved by fluorescence, the antenna can be used to construct a wide FOV optical concentrator.

Fig. 1 also illustrates how two different fluorescent antennas can be configured to support WDM transmission. In this example, each fluorescent antenna selectively absorbs the light transmitted from one transmitter, and the emitted light within each antenna is then guided to its associated photodetector. Consequently, two parallel transmission channels can be established. However, Fig. 1 represents an ideal scenario where each fluorescent antenna exclusively absorbs light emitted from one specific transmitter without interfering with the light emitted by the second transmitter. However, in practical applications, particularly in LED-based VLC systems, achieving this level of selectivity can be very challenging due to factors such as the broad emission spectrum of the light source, the broad absorption spectrum of the fluorophore, and the limited choice of available fluorophores. As a result, crosstalk between different channels is likely to occur. In the next section, we provide further insights into this crosstalk problem by introducing the spectra of the LEDs and the fluorescent fibers we used in this work.

B. Transmission Crosstalk

In this work, a luminaire was created using three different Lumileds LEDs: a blue LED (LXML-PR02-A900), a green LED (LXML-PM01-0100), and a red LED (LXM2-PD01-0050). The DC currents driving these LEDs were adjusted to produce white light suitable for typical indoor lighting. Fig. 2(a) shows the measured optical spectrum of the light emitted by this luminaire and Fig. 2(b) presents the associated CIE 1931 coordinates. Also, it can be obtained that the correlated color temperature (CCT) of

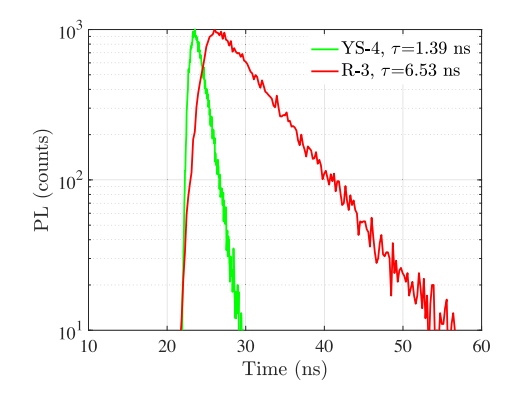


Fig. 3. Measured PL decay plots of the Kuraray YS-4 and R-3 fibers.

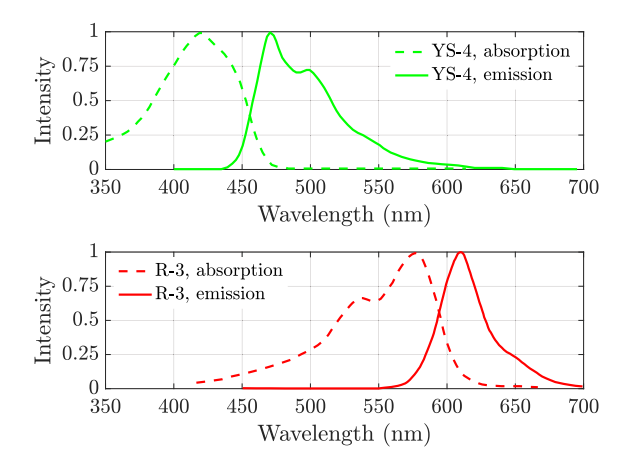


Fig. 4. Absorption and emission spectrum of the Kuraray YS-4 and R-3 fiber.

the emitted light is 7086 K, which is considered as "cool white" and suitable for illumination in many indoor environments. In our specific transmission configuration, the blue and green LEDs are set up to transmit two independent data streams, while the red LED is only powered by a DC current, enabling the output light to be white.

At the receiver, we considered commercially available fluorescent fibers manufactured by Kuraray to construct the optical antennas. One important reason for choosing Kuraray's fluorescent fibers is their remarkably short PL lifetime. Fig. 3 shows the measured PL decay results of the considered YS-4 and R-3 fiber using a streak camera system (Hamamatsu, C4780). The results show that their PL lifetimes are only 1.39 ns and 6.53 ns, respectively. Given that the 3 dB bandwidth of a fluorescent antenna can be calculated using

$$f_{3 \, \mathrm{dB}} = \frac{1}{2\pi\tau},\tag{1}$$

where τ is the PL lifetime [16], the 3 dB bandwidth of the YS-4 fiber antenna is therefore 72 MHz, and the 3 dB bandwidth of the R-3 fiber antenna is 15.3 MHz. These values are significantly higher compared to the bandwidth of a typical LED. Consequently, these antennas would not limit the bandwidth of the system. Another important characteristic of the fluorescent fiber lies in their absorption and emission spectra, shown in Fig. 4.

As explained, one fluorophore should have strong absorption of the light emitted by the blue LED, while the second fluorophore should strongly absorb the light emitted by the green LED. This is another reason why we chose the Kuraray YS-4 and R-3 fluorescent fibers. Comparing Fig. 4 with Fig. 2(a), it can be seen that the YS-4 fiber strongly absorbs the light emitted by the blue LED while completely avoiding the absorption of the light emitted by the green LED. In the case of the R-3 fiber, while it efficiently absorbs light from the green LED, there is also some absorption of light from the blue LED. Although it would be ideal if the second fluorophore only absorbs light emitted by the green LED, selecting fluorophores that completely avoid absorbing blue light is quite challenging due to the higher energy levels of the blue photons. This challenge is particularly pronounced when considering commercially available products which have limited options. To the best of our knowledge, when fluorescent antennas are employed for WDM, channel crosstalk is so far unavoidable [17], [18]. Fortunately, this crosstalk effect can be well mitigated using DSP methods. This involves treating the channels as a matrix, enabling the separation of signals by computing the inverse of the channel matrix. Consequently, the key challenge lies in selecting a fluorophore capable of creating a well-conditioned channel matrix with high singular values or eigenvalues so that the inverse of the channel matrix can be computed with good accuracy. In this work, since two LED transmitters and two photodetectors are used, the channel can be represented by a two-by-two matrix with each column corresponding to an LED transmitter and each row corresponding to a photodetector. If only optical power is considered [17], [18], the channel matrix after normalization is given by

$$\mathbf{H} = \begin{bmatrix} 1 & 0 \\ 0.85 & 0.81 \end{bmatrix}. \tag{2}$$

In (2), each element's value is determined by the optical power of the light emitted from the associated LED and the subsequent absorption and re-emission of light by the corresponding fluorescent fiber. As (2) is a triangular matrix, it is generally considered well-conditioned. In this case, its singular values are $\sigma_1=0.5643$ and $\sigma_2=1.4353$. Notably, these values are higher than the singular values of the channel matrix reported in [17] ($\sigma_1=0.5581$, $\sigma_2=1.3532$) and [18] ($\sigma_1=0.2535$, $\sigma_2=1.2827$). To clearly compare the two considered fluorescent fibers, their main parameters, including the peak and the full width at half maximum (FWHM) of the absorption and emission spectra, are summarized in Table I.

C. Imbalanced Channels

In LED-based VLC systems, the performance of the transmission is often limited by the bandwidth of the LEDs [3]. Fig. 5 shows the measured frequency response of the blue and green LEDs used in this work. It can be seen that the two LEDs have very different frequency responses. In particular, the blue LED has a 3 dB bandwidth of 4.5 MHz while the green LED's 3 dB bandwidth is only 2 MHz. To verify that the use of fluorescent antennas doesn't impact the bandwidth of this system, we also

 $\label{eq:table_interpolation} TABLE\ I$ Optical Properties of YS-4 and R-3 Fibers

	YS-4	R-3
Peak (abs.)	420 nm	577 nm
Peak (em.)	$470~\mathrm{nm}$	610 nm
FWHM (abs.)	68 nm	$75~\mathrm{nm}$
FWHM (em.)	56 nm	$35~\mathrm{nm}$
PL lifetime	1.39 ns	6.53 ns
Core refractive index	1.59	1.59
Cladding refractive index	1.49	1.49

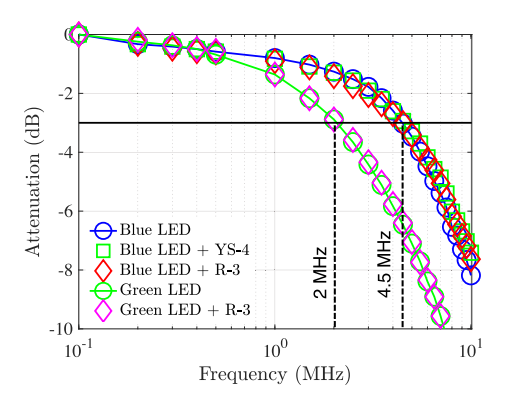


Fig. 5. Frequency response measured using the blue LED transmitter and the green LED transmitter, both with and without placing the fluorescent antenna in front of the photodetector.

measured the frequency response of the system when different antennas were used. In the case of the blue LED transmitter, both the YS-4 and R-3 fiber antennas were considered since both antennas absorb the blue light. In the case of the green LED transmitter, only the R-3 fiber antenna was considered, as the YS-4 fiber does not absorb the light emitted from the green LED. As expected, the use of antennas in our system has negligible impacts on the system's frequency response, thanks to the short PL lifetime of the fluorophores. These results also indicate that the transmission bandwidth of the system is dominated by the bandwidths of the LEDs. Also, the different frequency responses of the LEDs mean that the channel coefficient between each LED and each photodetector would vary at different frequencies. When OFDM is used as the modulation method, this means that the channel matrix would vary across different OFDM subcarriers. Therefore, to more accurately separate the signals, a distinct channel matrix should be obtained for each OFDM subcarrier. Moreover, the different received optical power by different photodetectors, combined with the differences in the frequency response of the LEDs, can lead to significant performance imbalances across the transmission channels. Similar to other multiplexing transmission systems, the system's overall performance is typically determined by its weakest channel. Therefore, implementing DSP methods to balance the performance across channels can significantly benefit the overall system.

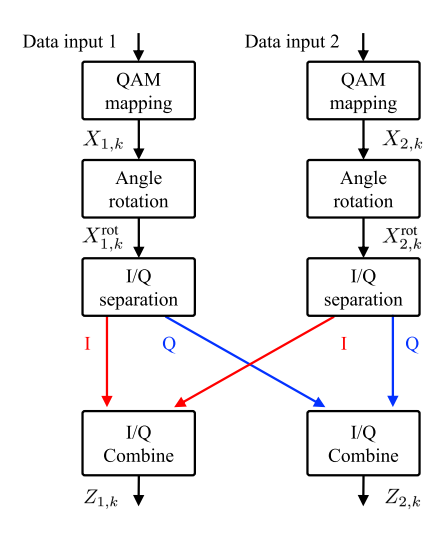


Fig. 6. Signal processing steps in a PWC encoder.

III. PWC IN WDM BASED VLC

The above described problem motivates the investigation into the use of PWC to deal with the impact of the performance imbalance. The underlying concept of PWC is to transfer the channel imbalance to the in-phase and quadrature components of the transmitted quadrature amplitude modulation (QAM) symbols and thereby enhancing overall performance. In this section, we provide a description of the structures of the investigated PWC encoder and decoder.

A. PWC Encoding

At the transmitter, the binary information bits are first converted to conventional QAM symbols using Gray coding. Since two LEDs are used for data transmission, two QAM symbols, $\mathbf{X}_k = [X_{1,k}, X_{2,k}]$, are first generated and then sent into a PWC encoder, as shown in Fig. 6. The PWC encoder produces two outputs, $\mathbf{Z}_k = [Z_{1,k}, Z_{2,k}]$, each of which is then loaded onto the kth subcarrier of the OFDM signal transmitted by a LED transmitter. To obtain \mathbf{Z}_k , both $X_{1,k}$ and $X_{2,k}$ are first rotated with an angle of ϕ as

$$\begin{cases} X_{1,k}^{\text{rot}} = X_{1,k} e^{i\phi} \\ X_{2,k}^{\text{rot}} = X_{2,k} e^{i\phi}. \end{cases}$$
 (3)

I/Q interleaving is then applied to give

$$\begin{cases} Z_{1,k} = \Re(X_{1,k}^{\text{rot}}) + i\Re(X_{2,k}^{\text{rot}}) \\ Z_{2,k} = \Im(X_{1,k}^{\text{rot}}) + i\Im(X_{2,k}^{\text{rot}}). \end{cases}$$
(4)

where $\Re(\cdot)$ and $\Im(\cdot)$ give the the real part and imaginary part of a complex value respectively and $i=\sqrt{-1}$ is the imaginary unit. The use of constellation rotation and I/Q interleaving means that the two QAM symbols, $\mathbf{X}_k = [X_{1,k}, X_{2,k}]$, which if transmitted without PWC will exhibit different performance, are now combined so that balanced performance across both channels can be achieved. The rotation step in (3) is intended to minimize the BERs for the balanced channels. In previous studies on PWC [21], [22], it was shown that fixing ϕ at 45° is a nearly

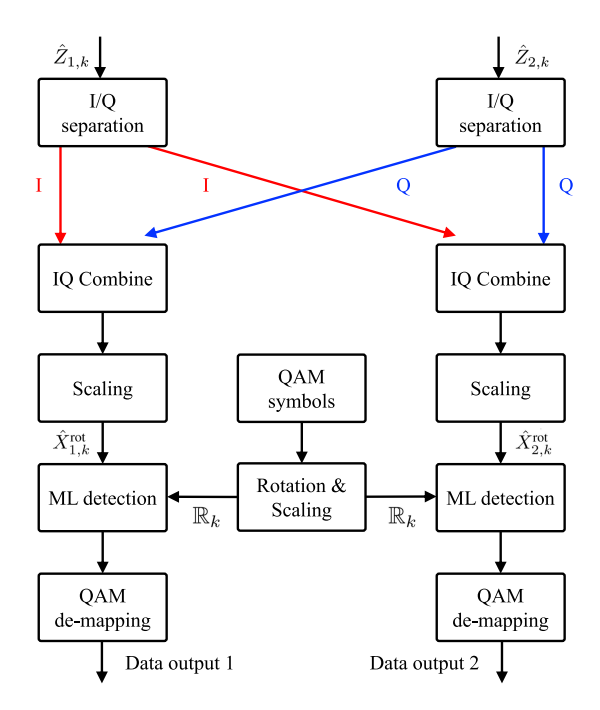


Fig. 7. Signal processing steps in a PWC decoder.

optimal choice. Although ϕ can be theoretically optimized based on the SNR difference between the two channels, optimizing the rotation angle is a complex task and can significantly increase system complexity while yielding only marginal performance improvements [22]. In this work, due to these considerations, ϕ is fixed at 45°. Next, to generate real-time domain signals suitable for IM/DD transmission, both $\mathbf{Z}_1 = [Z_{1,0}, Z_{1,1}, \ldots, Z_{1,N-1}]$ and $\mathbf{Z}_2 = [Z_{2,0}, Z_{2,1}, \ldots, Z_{2,N-1}]$ are constrained to have Hermitian symmetry, such that $Z_{1,k} = Z_{1,N-k}^*$ and $Z_{2,k} = Z_{2,N-k}^*$ for 0 < k < N/2, where N is the number of subcarriers [25]. Finally, both \mathbf{Z}_1 and \mathbf{Z}_2 are transformed into time-domain signals using IFFTs. Each of the obtained two signals is used to drive one of the data-transmitting LEDs.

B. PWC Decoding

At the receiver, the received signal on the kth subcarrier is given by

$$\mathbf{Y}_k = \mathbf{H}_k \mathbf{Z}_k + \mathbf{N}_k,\tag{5}$$

where \mathbf{H}_k is the 2×2 channel matrix associated with the kth subcarrier and \mathbf{N}_k is the noise component. Then, the signals transmitted from different LEDs need to be separated to avoid the crosstalk effect. In line with other related work [17], [18], we considered zero-forcing (ZF) equalizers, and the signals transmitted by two different LEDs are therefore separated using

$$\hat{\mathbf{Z}}_k = \hat{\mathbf{H}}_k^{-1} \mathbf{Y}_k. \tag{6}$$

where $\hat{\mathbf{H}}_k$ is the estimation of the channel matrix, \mathbf{H}_k . Next, as shown in Fig. 7, I/Q de-interleaving is applied to $\hat{\mathbf{Z}}_k$, followed by scaling the output using the singular values of $\hat{\mathbf{H}}_k$, $\sigma_{1,k}$ and

 $\sigma_{2,k}$ [23]. The processed results are given by

$$\begin{cases} \hat{X}_{1,k}^{\text{rot}} = \sigma_{1,k} \Re(\hat{Z}_{1,k}) + \sigma_{2,k} i \Re(\hat{Z}_{2,k}) \\ \hat{X}_{2,k}^{\text{rot}} = \sigma_{1,k} \Im(\hat{Z}_{1,k}) + \sigma_{2,k} i \Im(\hat{Z}_{2,k}). \end{cases}$$
(7)

At the following step, to obtain the reference points for performing data demodulation, each element within a M-QAM symbols set is first rotated by an angle of ϕ and then scaled based on the singular values of $\hat{\mathbf{H}}_k$ [23] to give

$$R_k = \sigma_{1,k} \Re(X e^{i\phi}) + \sigma_{2,k} i \Im(X e^{i\phi}), \tag{8}$$

where X is an element from a M-QAM constellation symbol set and R_k is one reference point belonging to the set, \mathbb{R}_k , used for performing decisions.

Finally, the signal is demodulated based on the maximum likelihood (ML) principle by finding the reference point to $\hat{X}_{1,k}^{\rm rot}$ or $\hat{X}_{2,k}^{\rm rot}$ with the shortest Euclidean distance as

$$\begin{cases}
\hat{R}_{1,k} = \underset{R_k \in \mathbb{R}_k}{\operatorname{argmin}} \{ ||\hat{X}_{1,k}^{\text{rot}} - R_k||^2 \} \\
\hat{R}_{2,k} = \underset{R_k \in \mathbb{R}_k}{\operatorname{argmin}} \{ ||\hat{X}_{2,k}^{\text{rot}} - R_k||^2 \}.
\end{cases}$$
(9)

Since $\hat{R}_{1,k}$ and $\hat{R}_{2,k}$ are paired with original QAM symbols, they can be directly demodulated into binary bits to recover the transmitted data.

C. Computational Complexity of PWC

Next, we discuss the computational complexity introduced by the use of PWC. To simplify the analysis, we also show that both the PWC encoder and the PWC decoder can be implemented through matrix multiplication. The processing steps of the PWC encoder, as shown in Fig. 6, involve a rotation step and an I/Q interleaver step. These two steps can be implemented together as a single matrix multiplication, as given by

$$\begin{bmatrix} \Re(Z_{1,k}) & \Im(Z_{1,k}) \\ \Re(Z_{2,k}) & \Im(Z_{2,k}) \end{bmatrix} = \begin{bmatrix} \cos \phi & -\sin \phi \\ \sin \phi & \cos \phi \end{bmatrix} \begin{bmatrix} \Re(X_{1,k}) & \Re(X_{2,k}) \\ \Im(X_{1,k}) & \Im(X_{2,k}) \end{bmatrix}$$
(10)

Since computing each element of the resulting matrix involves 2 multiplications and 1 addition, and there are four elements in the resulting matrix, the total number of operations includes 8 multiplications and 4 additions. Moreover, considering that N/2-1 subcarriers are used for data transmission, the overall additional operations include $8\times (N/2-1)$ multiplications and $4\times (N/2-1)$ additions compared to the transmitter without PWC. At the receiver side, the use of the PWC decoder also demands very low computational complexity. For instance, the I/Q de-interleaving step can be expressed as

$$\begin{bmatrix} \hat{X}_{1,k}^{\text{rot}} \\ \hat{X}_{2,k}^{\text{rot}} \end{bmatrix} = \begin{bmatrix} \sigma_{1,k} & \sigma_{2,k} \end{bmatrix} \begin{bmatrix} \Re(Z_{1,k}) & \Im(Z_{1,k}) \\ \Re(Z_{2,k}) & \Im(Z_{2,k}) \end{bmatrix}$$
(11)

Since this step involves 4 multiplications and 2 additions, the overall operations include $4 \times (N/2-1)$ multiplications and $2 \times (N/2-1)$ additions. Other processing steps, such as the singular value decomposition operation used to obtain the singular values, as well as the rotation step of the QAM constellation

symbols to obtain the decision reference points, need to be executed only once before data transmission. Consequently, their computational complexity is negligible.

When the transmission system includes more than two channels, multiple layers of PWC, as described in [26], can be implemented to balance performance across all channels. In this case, the computational complexity of implementing PWC increases and depends on both the number of layers and the number of channels. However, in contrast to other approaches for balancing channel performance, such as power allocation based methods [27], the incorporation of PWC into our system does not require channel information at the transmitter side. Moreover, since it involves only several steps of matrix multiplication, its computational complexity would be kept very low. More importantly, in comparison to the power allocation based approach, the use of PWC in multicolor LED based VLC does not affect the optical power of individual LEDs. Consequently, it does not impact the spectrum of the transmitter, which is required to provide white light suitable for indoor illumination.

IV. CHANNEL ESTIMATION AND EQUALIZATION

As explained in the previous sections, the channel matrix associated with each OFDM subcarrier, H_k , is required to be pre-estimated. In this section, we introduce a new structure of the transmitted signals which enables the estimation of all elements within the channel matrix for all OFDM subcarriers without encountering interference. Moreover, compared to the conventional time domain based channel estimation approach [28], in which each LED needs to be turned off to transmit a sequence of zeros to avoid interference between the pilot symbols transmitted from two LEDs, this new frequency domain based approach keeps all LEDs on continuously. Consequently, the instantaneous light intensity is more stable, and the lighting quality is less affected. Fig. 8 shows the structure of the signals transmitted from both LEDs. Initially, two sequences of $N_{\rm pilot}$ pilot symbols are transmitted. These symbols are used for channel estimation before any data transmission takes place. The details of the pilot symbols are shown in Fig. 8(c) and (d). In pilot symbol, $P_{\rm A}$, known QAM values are transmitted on odd frequency subcarriers, $I_{\text{odd}} = 1, 3, 5, \dots, N-1$, and the even subcarriers, $I_{\text{even}} = 2, 4, 6, ..., N - 2$, are set to zeros. While for the pilot symbol, $P_{\rm B}$, known QAM values are transmitted on the even frequency subcarriers and the odd subcarriers are set to zeros. Transmission begins with a sequence of N_{pilot} pilot symbols P_{A} being sent from LED1. Simultaneously, a sequence of $N_{\rm pilot}$ pilot symbols $P_{\rm B}$ is sent from LED2. The use of different subcarriers on the two LEDs allows these subcarriers to be demodulated without inter-channel interference. Next, another sequence of $N_{\rm pilot}$ symbols is transmitted, but this time, symbol $P_{\rm B}$ is sent from LED1 and symbol P_A is sent from LED2. The design of the pilot sequences means that, by the end of the transmission of pilot signals, each LED has transmitted pilot symbols on all subcarriers. Also, note that because the transmission of the pilot symbols is intended for estimating the channel coefficients, unlike the symbols generated for data transmission, PWC is not implemented for these pilot symbols. In this case, the received

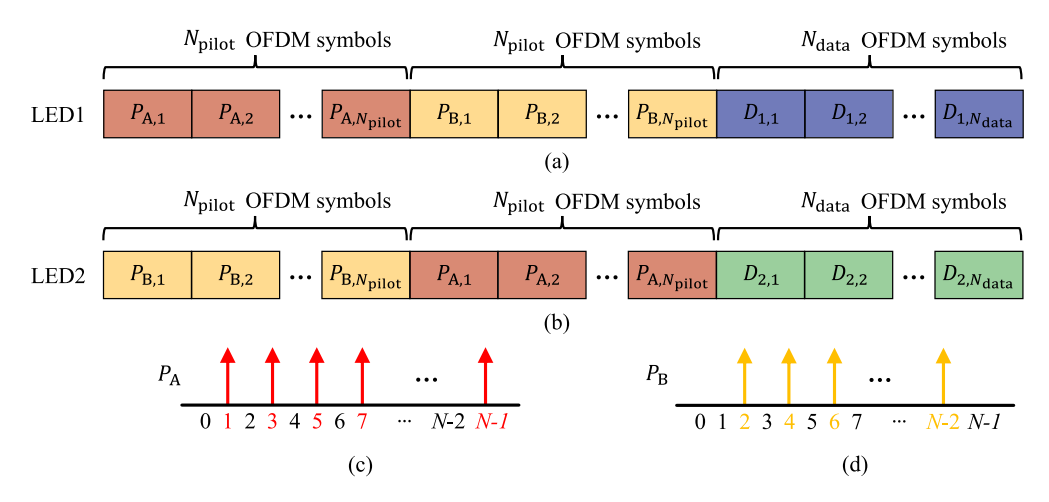


Fig. 8. Schematic diagram of the transmitted signals, (a) signals transmitted from the blue LED, (b) signals transmitted from the green LED, (c) pilot symbol structure of $P_{\rm A}$, (d) pilot symbol structure of $P_{\rm B}$.

signal vector on the kth OFDM subcarrier, $\mathbf{Y}_k = [Y_{1,k}, Y_{2,k}]$, can be expressed as

$$\mathbf{Y}_k = \mathbf{H}_k \mathbf{X}_k + \mathbf{N}_k \tag{12}$$

where $\mathbf{X}_k = [X_{1,k}, X_{2,k}]$ is the transmitted pilot QAM symbol vector. In particular, during the first pilot sequence transmission, the received signals on I_{odd} subcarriers are given by

$$\begin{bmatrix} Y_{1,I_{\text{odd}}} \\ Y_{2,I_{\text{odd}}} \end{bmatrix} = \begin{bmatrix} H_{11,I_{\text{odd}}}, H_{12,I_{\text{odd}}} \\ H_{21,I_{\text{odd}}}, H_{22,I_{\text{odd}}} \end{bmatrix} \begin{bmatrix} X_{1,I_{\text{odd}}} \\ 0 \end{bmatrix} + \begin{bmatrix} N_{1,I_{\text{odd}}} \\ N_{2,I_{\text{odd}}} \end{bmatrix}$$
(13)

Since N_{pilot} pilot symbols are transmitted in each pilot sequence, the channel can be estimated as $\hat{H}_{11,I_{\mathrm{odd}}} = \frac{1}{N_{\mathrm{pilot}}} \sum_{n=1}^{N_{\mathrm{pilot}}} \frac{Y_{1,I_{\mathrm{odd}}}(n)}{X_{1,I_{\mathrm{odd}}}(n)}$, $\hat{H}_{21,I_{\mathrm{odd}}} = \frac{1}{N_{\mathrm{pilot}}} \sum_{n=1}^{N_{\mathrm{pilot}}} \frac{Y_{2,I_{\mathrm{odd}}}(n)}{X_{1,I_{\mathrm{odd}}}(n)}$ for all odd subcarriers. Similarly, the received signals on the even subcarriers are given by

$$\begin{bmatrix} Y_{1,I_{\text{even}}} \\ Y_{2,I_{\text{even}}} \end{bmatrix} = \begin{bmatrix} H_{11,I_{\text{even}}}, H_{12,I_{\text{even}}} \\ H_{21,I_{\text{even}}}, H_{22,I_{\text{even}}} \end{bmatrix} \begin{bmatrix} 0 \\ X_{2,I_{\text{even}}} \end{bmatrix} + \begin{bmatrix} N_{1,I_{\text{even}}} \\ N_{2,I_{\text{even}}} \end{bmatrix}$$

$$\uparrow \qquad \qquad \uparrow \qquad \qquad \downarrow \qquad \qquad \uparrow \qquad \qquad \downarrow \qquad \qquad \downarrow$$

 $\text{Therefore, } \hat{H}_{12,I_{\text{even}}} = \frac{1}{N_{\text{pilot}}} \sum_{n=1}^{N_{\text{pilot}}} \frac{Y_{1,I_{\text{even}}}(n)}{X_{2,I_{\text{even}}}(n)} \text{ and } \hat{H}_{22,I_{\text{even}}} =$

 $\frac{1}{N_{\rm pilot}} \sum_{n=1}^{N_{\rm pilot}} \frac{Y_{2,I_{\rm even}}(n)}{X_{2,I_{\rm even}}(n)} \ \ {\rm can\ be\ obtained.} \ \ {\rm In\ the\ second\ pilot} \ \ {\rm sequence\ transmission,\ similar\ to\ the\ above\ calculations,\ the\ received\ {\rm signal\ can\ be\ used\ to\ estimate} \ H_{12,I_{\rm odd}},\ H_{22,I_{\rm odd}},\ H_{11,I_{\rm even}},\ H_{21,I_{\rm even}}. \ \ {\rm Consequently,\ the\ channel\ estimation\ is\ completed\ after\ the\ second\ pilot\ sequence\ transmission\ and\ the\ estimated\ channel,\ \hat{\mathbf{H}}_k,\ {\rm can\ be\ used\ to\ separate\ signals\ received\ in\ the\ data\ sequence\ transmission.}$

V. EXPERIMENTAL SETUP

The block diagram of our experimental setup is shown in Fig. 9. The two signal sequences intended for transmission, generated using the method described in the above section, were first obtained offline using Matlab. Subsequently, these two signals were uploaded into an arbitrary waveform generator (AWG, Siglent SDG2082X), with each signal occupying one

channel. To drive a LED transmitter, each signal output from the AWG was first amplified through a power amplifier (Minicircuits, ZHL-32A-S) and then superimposed onto a DC signal using a bias-T (Mini-circuits, ZFBT-4R2GW). As explained, in this work, we configured a blue LED (Lumileds, LXML-PR02-A900) and a green LED (Lumileds, LXML-PM01-0100) to transmit two independent data streams. The red LED (Lumileds, LXM2-PD01-0050) was directly powered by a DC signal. These three LEDs were closely placed and soldered onto an aluminium PCB board (SinkPAD-II, Tri-Star base). To spatially mix the light emitted from these three LEDs, an optical diffuser was placed in front of the luminaire.

At the receiver, as shown in Fig. 10, each antenna consisted of two bent fluorescent fibers and was coupled with an avalanche photodetector (APD, Thorlabs, APD130 A). The length of each fiber was considered to be 35 cm. The benefit of considering this shape of the antenna is that it can receive incident light from most directions and the antenna is close to omnidirectional [6], [29]. Fig. 10 also shows the appearance of these two antennas when illuminated by both the blue LED and the green LED. It can be seen that both antennas fluoresce under the illumination the blue LED. This is because, as explained in Section II, both antennas can absorb the emitted light of the blue LED. This allows both APDs to receive the signal transmitted from the blue LED. Furthermore, it can be seen from Fig. 10(b) that when exposed to the green LED, the YS-4 fiber becomes transparent, while the R-3 fiber emits red light. This means, as expected, that only one APD can detect light emitted from the green LED. This observation intuitively demonstrates why the channel in our WDM system can be represented as a triangular matrix. Finally, for both APDs, their output signals were captured using an oscilloscope (DSO, LeCroy, 204Xi-A). They were then processed offline to recover the transmitted data.

VI. TRANSMISSION PERFORMANCE

In this section, we analyze the system's performance by showing the measured results, including the concentration gain of the antennas, the estimated channels, the received constellations, and BERs at various illuminance levels. Furthermore,

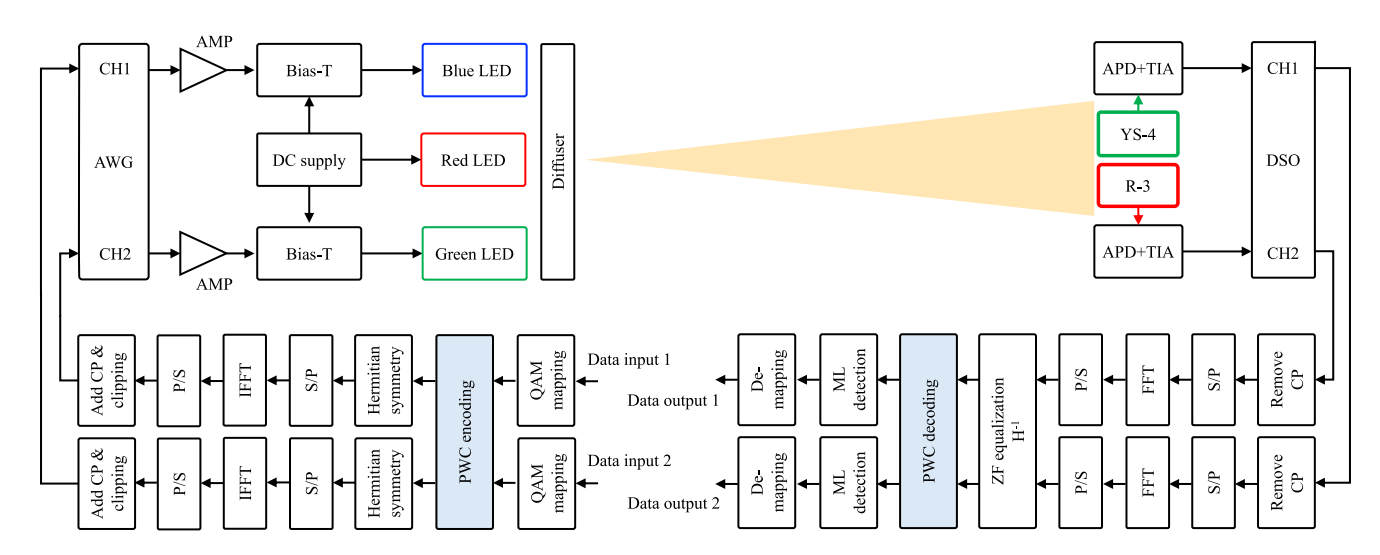


Fig. 9. Block diagram of the transmission system.

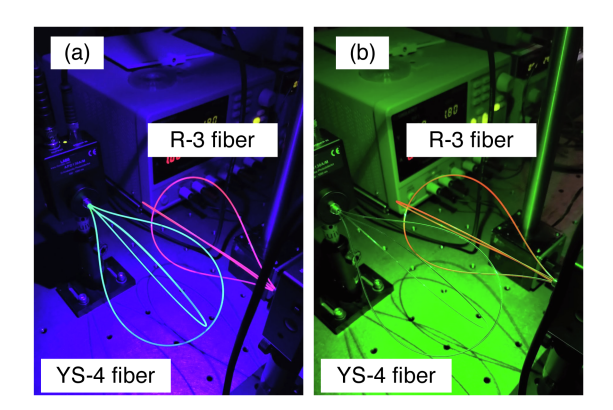


Fig. 10. Photos of the antennas (a) under blue LED light, (b) under green LED light.

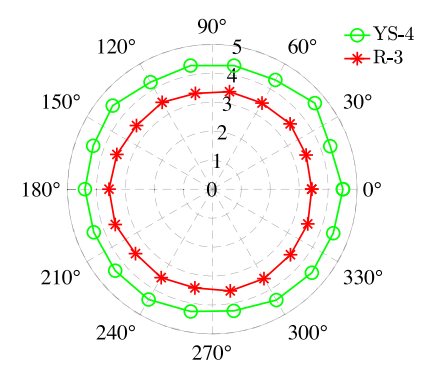


Fig. 11. Measured concentration gain by rotating the antennas with different angles.

we highlight the benefits of employing PWC in the system by comparing the measured results with and without its usage.

A. Concentration Gain

Typically, the gain of an optical concentrator is defined as the ratio of the collected optical power with and without the concentrator. However, in VLC systems, the received signal strength is influenced not only by the number of photons arriving at the photodetector, which is directly related to the optical power of the light, but also by the wavelengths of the photons emitted from the antenna and whether these wavelengths are sensitive to the used Si photodetector. Consequently, we define the antenna's gain as the ratio of received electrical signal strength, measured in peak-to-peak voltage, with and without the antenna, while transmitting a 500 KHz sine wave. For the antenna constructed from YS-4 fibers, we used the blue LED as the transmitter. In contrast, for the antenna made of R-3 fibers, we used the green LED as the transmitter. Moreover, the gain was measured when the antenna was mounted onto a rotation stage (Thorlabs, RSP1D/M) with a SMA fiber adapter (Thorlabs, SM1SMA) so

that we could measure the gains at different polar angles of the incident light. Fig. 11 shows the measured results. It can be seen that the YS-4 antenna and the R-3 antenna provide a gain of approximately 4.5 and 3.5 respectively. Moreover, the gains remained the same when the antenna was rotated. Since the gain is defined as the ratio by which the amplitude of the electrical signal is amplified, a gain of approximately 4 means that the power of the received electrical signal is increased by a factor of approximately 16. This is equivalent to a 12 dB improvement in SNR compared to using bare photodetectors. According to the inverse-square law, an increase in signal strength by a factor of 4 means that, to maintain the same signal strength or the optical power, the transmission distance can be doubled. In practical applications, higher gains can be achieved through strategies such as increasing the fiber length [30], employing multiple fibers [6], improving the coupling efficiency between the fibers and the APD, or developing fluorescent antennas with a large Stokes shift since a large Stokes shift can mitigate the self-absorption effect and also means that the emitted wavelengths are even longer, making them more sensitive to Si photodetectors.

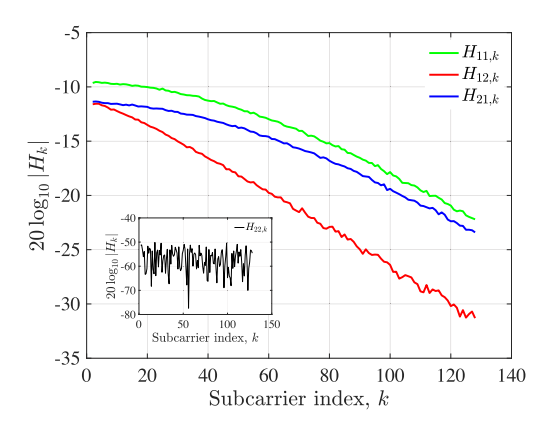


Fig. 12. Estimated channel response of four channels when the transmission sampling rate is 20 MSa/s per channel and the illuminance level at the receiver is 560 lx.

B. The WDM Channels

Fig. 12 shows the estimated channels using the method described in Section IV. In this example, the transmission sampling rate was fixed at 20 MSa/s and the illuminance level at the receiver was 560 lx which is associated with a transmission distance of 0.5 m. In these plots, the channel coefficients associated with the signal transmitted by the blue LED, denoted as $H_{11,k}$ and $H_{21,k}$, have very similar shapes. This is because both the shapes of these plots are determined by the frequency response of the blue LED. Also, despite our APDs being more sensitive to red light than green light, $H_{21,k}$ has lower values than $H_{11,k}$ due to the significantly lower absorption of blue light in the R-3 fiber compared to the YS-4 fiber. $H_{12,k}$ and $H_{22,k}$ are the channel coefficients between the green LED and the two APDs, respectively. When comparing $H_{12,k}$ with $H_{21,k}$, it can be seen that the channel coefficients have very similar values for the low-frequency subcarriers. However, as the subcarrier index or frequency increases, $H_{12,k}$ starts to have lower values compared to $H_{21,k}$. This difference is attributed to the frequency response difference between the blue LED and the green LED, as shown in Fig. 5. The lower bandwidth of the green LED leads to lower values of $H_{12,k}$ in comparison to $H_{21,k}$. Finally, since the YS-4 fiber does not absorb the light emitted from the green LED, $H_{22,k}$ contains only noise.

C. The Received Constellations

To clearly show the benefits of using PWC in our system, we present Figs. 13 and 14 to show the received signal constellations without and with PWC under identical transmission conditions. In these examples, the constellations were obtained at a transmission data rate of 4 Mbps per channel and an illuminance level of $560\,\mathrm{lx}$ at the receiver. Fig. 13 reveals distinct differences between the two channels when no PWC is employed. In particular, Fig. 13(a) shows that the received signal which is transmitted by the blue LED has a relatively low noise level, resulting in a BER of 0. On the other hand, Fig. 13(b) show that the signal transmitted by the green LED is received with a higher noise level, leading to a BER of 2.13×10^{-4} . In this case, the overall

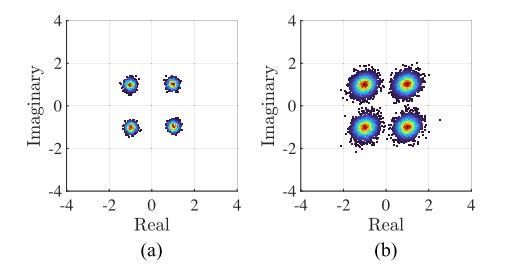


Fig. 13. Received 4-QAM constellations without PWC when the data rate is 4 Mbps per channel, (a) the blue LED channel, (b) the green LED channel.

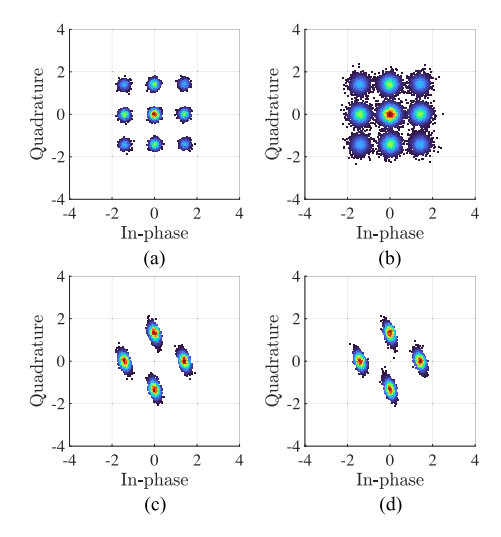


Fig. 14. Received 4-QAM constellations with PWC when the data rate is 4 Mbps per channel, (a) the blue LED channel before I/Q de-interleaving, (b) the green LED channel before I/Q de-interleaving, (c) the blue LED channel after I/Q de-interleaving, (d) the green LED channel after I/Q de-interleaving.

BER is 1.05×10^{-4} . Next, Fig. 14 is presented to demonstrate how employing PWC can mitigate the imbalance between the two channels. Fig. 14(a) and (b) show received constellations after channel equalization but before I/Q de-interleaving is implemented. Unlike the conventional 4-QAM, the transmitted constellation contains nine 'points' due to rotation and I/Q interleaving used in the PWC encoder. Before I/Q de-interleaving, it can be seen that the received signal experiences the same performance imbalance. However, this performance imbalance is significantly mitigated after implementing I/Q de-interleaving, as demonstrated in Fig. 14(c) and (d) that the two channels have always identical performance. Notably, in this example, both channels achieve a BER of 0.

D. Measured BERs

Next, we show the measured BERs when different transmission data rates were considered. In our experiment, the constellation was fixed at 4-QAM and different transmission data rates were achieved by varying the transmission sampling rate. Fig. 15(a) shows the results when no PWC was used and the illuminance level at the receiver was 560 lx. It can be seen that, as expected, the data transmitted by the green LED is

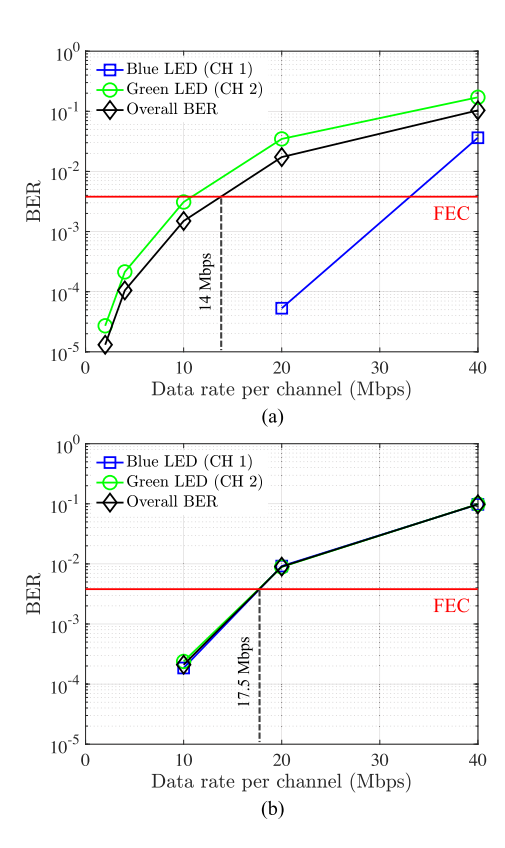


Fig. 15. Measured BERs at different transmission data rates when the illuminance level at the receiver is 560 lx, (a) without PWC and (b) with PWC.

always demodulated with much higher BERs compared to the data transmitted by the blue LED for all considered data rates. Moreover, it also shows that the overall BER is dominated by the performance of the green LED channel. Considering the 7% FEC limit of 3.8×10^{-3} , the achievable data rate was 14 Mbps per channel, resulting in an overall achievable data rate of 28 Mbps. Fig. 15(b) shows the measured results when PWC was used. It can be seen that the two channels have almost identical performance. Compared to Fig. 15(a), the achievable transmission data rate per channel is increased from 14 Mbps to 17.5 Mbps, and this means, by using PWC, the overall achievable transmission data rate is increased from 28 Mbps to 35 Mbps.

E. Different Illuminances

Also, the system's transmission performance was measured by varying the illuminance level at the receiver. This was achieved by changing the distance between the LED luminaire and the receiver. In particular, the transmission distance was increased from 0.5 m to 0.9 m, with each increment being 0.1 m. This caused the illuminance level to change from 560 lx to 170 lx so that different recommended illuminance levels in various indoor settings were considered. For each illuminance level, we measured the BERs at different transmission data rates and considered both cases without PWC and with PWC. Fig. 15 shows the result when the illuminance was 560 lx and Fig. 16(a)–(d) shows the results at illuminances of 390 lx, 280 lx, 220 lx, and 170 lx. As expected, the BER increases when the

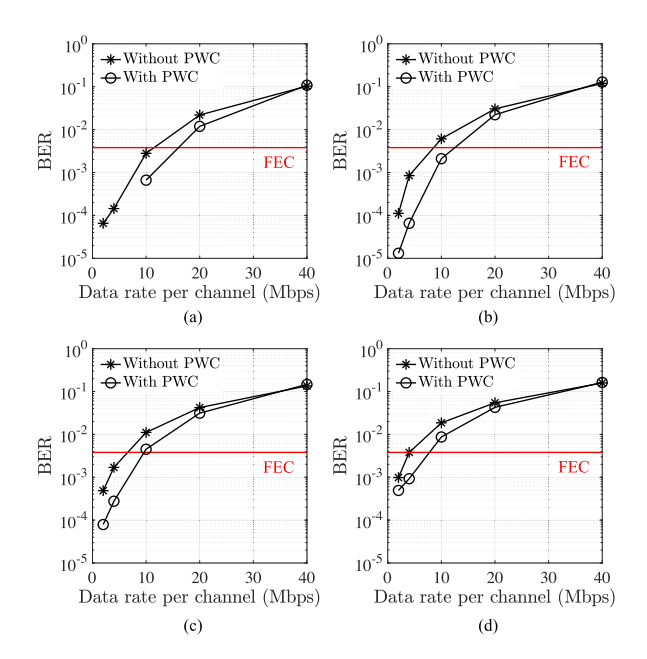


Fig. 16. Measured BER vs transmission data rate at different illuminances (a) 390 lx, (b) 280 lx, (c) 220 lx, (d) 170 lx.

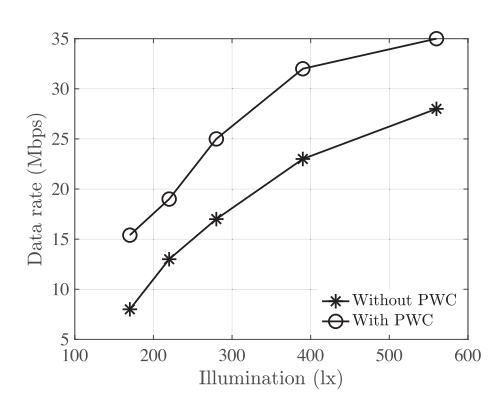


Fig. 17. Achievable transmission data rate at different illuminance levels with and without using PWC.

illuminance level at the receiver changes from high to low. Also, we can see that, regardless of the transmission data rate and the illuminance level, using PWC can always result in a lower BER. Based on the results shown in Figs. 15 and 16, we also obtained the data rate at which the BER equals the FEC limit for different illuminances and plot these results in Fig. 17. First, the results show that increasing the illuminance at the receiver can always result in a higher transmission data rate. Most notably, the use of PWC demonstrates a potential improvement of 5–10 Mbps in the achievable transmission data rate.

VII. CONCLUSION

The use of fluorescent optical antennas in VLC is very promising way for enhance the transmission performance. This is because these antennas can achieve both high optical concentration gains and wide FOVs without conserving the étendue limit. Also, their short PL lifetime means that they can support very high

transmission bandwidth. Moreover, since they are also capable of optical filtering, one very useful application is to employ them in supporting WDM transmission, which can significantly boost the data transmission rate. However, two notable challenges may arise. One is the crosstalk between different transmission channels, while the other is performance imbalances among the received data streams. In this paper, we verified these challenges through constructing a white light-based WDM VLC system, utilizing LEDs and fluorescent fibers which are all commercially available products. Moreover, to address the cross-talk effect, we have proposed a new channel estimation method that allows for the effective estimation of individual channel matrices for each OFDM subcarrier. Unlike previous approaches, these channel matrices not only consider the optical power 'leakage' between different channels but also include the frequency response of individual transmitters. Another significant contribution of this work is the incorporation of PWC in the transmission to balance the performance between the 'good' channels and the 'bad' channels. We have demonstrated the benefits of using PWC by measuring the system performance considering a range of typical illumination levels. The measured results show that employing PWC can always lead to substantial data rate improvements. Future work will involve developing antennas with even shorter PL lifetimes and testing the performance of these optical antennas with high-speed micro-LEDs or eye-safe lasers. Given that the PL lifetime can potentially dominate transmission bandwidth in such systems, differences in PL lifetimes among the fluorophores can lead to greater imbalances between channels. The use of PWC in such systems is anticipated to yield further benefits.

REFERENCES

- [1] A. Jovicic, J. Li, and T. Richardson, "Visible light communication: Opportunities, challenges and the path to market," *IEEE Commun. Mag.*, vol. 51, no. 12, pp. 26–32, Dec. 2013.
- [2] H. Haas, L. Yin, Y. Wang, and C. Chen, "What is LiFi?," J. Lightw. Technol., vol. 34, no. 6, pp. 1533–1544, Mar. 2016.
- [3] D. O'Brien, S. Rajbhandari, and H. Chun, "Transmitter and receiver technologies for optical wireless," *Philos. Trans. Roy. Soc. A*, vol. 378, no. 2169, 2020, Art. no. 20190182.
- [4] S. Collins, D. C. O'Brien, and A. Watt, "High gain, wide field of view concentrator for optical communications," *Opt. Lett.*, vol. 39, no. 7, pp. 1756–1759, 2014.
- [5] P. P. Manousiadis et al., "Wide field-of-view fluorescent antenna for visible light communications beyond the étendue limit," *Optica*, vol. 3, no. 7, pp. 702–706, 2016.
- [6] T. Peyronel, K. Quirk, S. Wang, and T. Tiecke, "Luminescent detector for free-space optical communication," *Optica*, vol. 3, no. 7, pp. 787–792, 2016.
- [7] Y. Dong et al., "Nanopatterned luminescent concentrators for visible light communications," *Opt. Exp.*, vol. 25, no. 18, pp. 21926–21934, 2017.
 [8] C. H. Kang et al., "Ultraviolet-to-blue color-converting scintillating-fibers
- [8] C. H. Kang et al., "Ultraviolet-to-blue color-converting scintillating-fibers photoreceiver for 375-nm laser-based underwater wireless optical communication," *Opt. Exp.*, vol. 27, no. 21, pp. 30450–30461, 2019.
- [9] M. A. Umair et al., "Long-range optical wireless communication system based on a large-area, Q-Dots fluorescent antenna," *Laser Photon. Rev.*, vol. 17, no. 2, 2022, Art. no. 2200575.

- [10] C. He and S. Collins, "A two-stage fluorescent antenna for visible light communication uplinks," *IEEE Photon. Technol. Lett.*, vol. 35, no. 21, pp. 1190–1193, Nov. 2023.
- [11] C. H. Kang et al., "All-inorganic halide-perovskite polymer-fiber-photodetector for high-speed optical wireless communication," *Opt. Exp.*, vol. 30, no. 6, pp. 9823–9840, 2022.
- [12] C. He, Y. Lim, and H. Murata, "Study of using different colors of fluorescent fibers as optical antennas in white led based-visible light communications," *Opt. Exp.*, vol. 31, no. 3, pp. 4015–4028, 2023.
- [13] S. Alshaibani et al., "Wide-field-of-view optical detectors for deep ultraviolet light communication using all-inorganic CsPbBr3 perovskite nanocrystals," Opt. Exp., vol. 31, no. 16, pp. 25385–25397, 2023.
- [14] Y. Wang et al., "Multifunctional difluoroboron β-diketonate-based luminescent receiver for a high-speed underwater wireless optical communication system," *Opt. Exp.*, vol. 31, no. 20, pp. 32516–32528, 2023.
- cation system," *Opt. Exp.*, vol. 31, no. 20, pp. 32516–32528, 2023. [15] C. He, S. Collins, and H. Murata, "Capillary-based fluorescent antenna for visible light communications," *Opt. Exp.*, vol. 31, no. 11, pp. 17716–17730, 2023.
- [16] M. Portnoi et al., "Bandwidth limits of luminescent solar concentrators as detectors in free-space optical communication systems," *Light: Sci. Appl.*, vol. 10, no. 1, 2021, Art. no. 3.
- [17] P. P. Manousiadis et al., "Optical antennas for wavelength division multiplexing in visible light communications beyond the étendue limit," *Adv. Opt. Mater.*, vol. 8, no. 4, 2020, Art. no. 1901139.
- [18] M. Sait et al., "Dual-wavelength luminescent fibers receiver for wide field-of-view, Gb/s underwater optical wireless communication," *Opt. Exp.*, vol. 29, no. 23, pp. 38014–38026, 2021.
- [19] E. Khorov and I. Levitsky, "Current status and challenges of Li-Fi: IEEE 802.11 bb," *IEEE Commun. Standards Mag.*, vol. 6, no. 2, pp. 35–41, Jun. 2022.
- [20] C. He, T. Q. Wang, and J. Armstrong, "Performance of optical receivers using photodetectors with different fields of view in a MIMO ACO-OFDM system," *J. Lightw. Technol.*, vol. 33, no. 23, pp. 4957–4967, Dec. 2015.
- [21] J. Boutros and E. Viterbo, "Signal space diversity: A power-and bandwidth-efficient diversity technique for the Rayleigh fading channel," *IEEE Trans. Inf. Theory*, vol. 44, no. 4, pp. 1453–1467, Jul. 1998.
- [22] C. Zhu, B. Song, B. Corcoran, L. Zhuang, and A. J. Lowery, "Improved polarization dependent loss tolerance for polarization multiplexed coherent optical systems by polarization pairwise coding," *Opt. Exp.*, vol. 23, no. 21, pp. 27434–27447, 2015.
- [23] H. G. Olanrewaju, J. Thompson, and W. O. Popoola, "Pairwise coding for MIMO-OFDM visible light communication," *IEEE Trans. Wireless Commun.*, vol. 19, no. 2, pp. 1210–1220, Feb. 2020.
- [24] B. Deng et al., "Polarization multiplexing based UOWC systems under bubble turbulence," *J. Lightw. Technol.*, vol. 41, no. 17, pp. 5588–5598, Sep. 2023.
- [25] S. D. Dissanayake and J. Armstrong, "Comparison of ACO-OFDM, DCO-OFDM and ADO-OFDM in IM/DD systems," *J. Lightw. Technol.*, vol. 31, no. 7, pp. 1063–1072, Apr. 2013.
- [26] J. Wang, C. Chen, B. Deng, Z. Wang, M. Liu, and H. Fu, "Enhancing underwater VLC with spatial division transmission and pairwise coding," *Opt. Exp.*, vol. 31, no. 10, pp. 16812–16832, 2023.
- [27] K.-H. Park, Y.-C. Ko, and M.-S. Alouini, "On the power and offset allocation for rate adaptation of spatial multiplexing in optical wireless MIMO channels," *IEEE Trans. Commun.*, vol. 61, no. 4, pp. 1535–1543, Apr. 2013.
- [28] Y. Wang and N. Chi, "Demonstration of high-speed 2x2 non-imaging MIMO nyquist single carrier visible light communication with frequency domain equalization," *J. Lightw. Technol.*, vol. 32, no. 11, pp. 2087–2093, Jun. 2014.
- [29] C. He, Y. Lim, Y. Tang, and C. Chen, "Visible light communications using commercially available fluorescent fibers as optical antennas," in *Proc. Opto- Electron. Commun. Conf.*, 2023, pp. 1–4.
- [30] W. Ali, Z. Ahmed, W. Matthews, and S. Collins, "The impact of the length of fluorescent fiber concentrators on the performance of VLC receivers," *IEEE Photon. Technol. Lett.*, vol. 33, no. 24, pp. 1451–1454, Dec. 2021.